Chapter 13

Evaluating Urban Heat Island Effects in Rapidly Developing Coastal Cities

Siqiang Wang, Meng Xiang, Yanan He, JinYeu Tsou, Yuanzhi Zhang, X. San Liang and Xia Lu

Additional information is available at the end of the chapter

http://dx.doi.org/10.5772/intechopen.80020

Abstract

In this chapter, we present the analysis of urban heat island (UHI) effects on coastal urban areas using satellite images as a case study in Hangzhou, China. With the sustainable development of coastal areas, land use and land cover have been dramatically changed. Such changes make the phenomenon of urban heat island (UHI) becoming serious, which has brought some negative influences on human activities or public health issues in coastal regions. This study takes Hangzhou as an example of coastal cities and uses the Landsat TM, ETM+ and OLI images to retrieve the urban land surface temperature (LST). We also mapped and compared the intensity of UHI effects in different years of 2003, 2008 and 2013. The result shows that the intensity of UHI effect in 2013 was more serious than previous years, which is increasing year by year. The study also analyzed the relationship between UHI, NDVI, and NDBI and provided some useful suggestions to mitigate the UHI effects on coastal cities such as Hangzhou in China.

Keywords: urban heat island, land surface temperature, normalized difference vegetation index, normalized difference build-up index

1. Introduction

Urban heat island (UHI), which means the temperature in urban and suburban area are higher than the surrounding rural area, has become the most significant phenomenon of climate change [1]. One important reason is that the urban land space once was moist and permeable that changed to dry and impervious surface after human activities [2]. With the continuous development and expansion of the city, this phenomenon gradually becomes more common,

especially in summer. The extreme temperature increases the energy consumption of city and causes respiratory diseases and other difficulties [3]. A fast and available monitoring of UHI effect has become particularly necessary. Remote sensing technology provides a continuous monitoring of urban heat island in a vast scope. The land surface temperature can be easily retrieved by using the thermal infrared wave band [4].

There has been a lot of research on remote sensing temperature retrieval. Senanayake et al. used the thermal band (band 6) images of a serious Landsat satellite to map the distribution of the land surface temperature of Colombo City [5]. Huang et al. carried out three different methods (one radiative transfer equation (RTE) method, two mono-window algorithm methods) to retrieve the land surface temperature and demonstrated that the accuracy of the temperature results retrieved by remote sensing data is acceptable compared with the actual temperature data [6]. Rinner and Hussain used Toronto as an example to explore the relationship between land use and urban environment; the vector data analysis (zonal statistics) and descriptive statistics along with an analysis of variance (ANOVA) were applied [7]. Chen et al. combined the statistic of population and economic to build a model, argued the correlation between the investigation of urbanization and urban heat island in Beijing [8]. They also used zonal statistics (raster grid analysis and regional analysis) and geostatistical tool in ArcGIS to compare the 2 years' data and found that there was a close relationship between the remote UHI and urbanization. Some studies focus on the urban heat island of big cities in China, such as Hong Kong [9], Wuhan [10], Shanghai [11], and so on. The research objectives in this chapter have been formulated as follows: (1) to compare the change of UHI intensity on the temporal and spatial level, (2) to define the relationship among UHI, vegetation and buildings.

Hangzhou, which is in Zhejiang province, China (30°15′0″N, 120°10′0″E), was selected as the study area in this research. In recent decades, the economic development in Hangzhou is very fast, which led to urban construction activities, once the rural land has now become an urban area. Besides, the weather is wet and extremely hot in summer, so it is necessarily to mitigate the urban heat island effect. The major city area is selected in this study, which contains eight districts, such as Gongshu, Shangcheng, Xiacheng, Jianggan, Xihu, Bingjiang, Yuhang, and Xiaoshan.

2. Methodology

2.1. Data collection

The Landsat TM, ETM+ and OLI data are used in this study. The historical meteorological data are also collected. Landsat Program is the most widely used and most effective remote sensing source, which is available on the USGS website [9]. In order to have a better image quality, there are some difficulties. First, good weather condition (mainly affected by cloud cover) is a must. Second, there is little data of each month, for the repeat interval of Landsat satellite is 16 days, which means only two image data per month at the same location. In addition, the Landsat 7 data after May 31, 2003 have not been used because the scan line corrector (SLC) has failed and made some data lost. Therefore, the data that can be used are very

http://dx.doi.org/10.5772/intechopen.80020

limited, so the chosen data are not on the same month. In that way, **Figure 1** illustrates the image data information (display in true color): March 26, 2003, ETM+; May 2, 2008, TM; April 14, 2013, OLI. All data are with little cloud cover to avoid interference.

2.2. Image preparation

Because of some inevitable interference, the data need to be processed before the analysis. First is to do radiometric calibration to correct the sensitivity of the remote sensor, topography, Sun angle, atmospheric scattering and absorption. Next is to do the geometric correction to make the image's projection precisely matches a specific projection surface or shape (here unified the projection of WGS_1984). Another important step is to do atmospheric correction to eliminate the error caused by atmospheric scattering, absorption and reflection, and the FLAASH is used in our study. Finally, it also needs to resample the image data because the resolution of the thermal band is different to other bands. The resolution of the thermal band of Landsat 5 (band 6) is 120 m, Landsat 7 (band 6) is 60 m, and Landsat 8 (bands 10 and 11) is 100 m, and the resolution of the rest other bands is 30 m. The result of the treatment is shown in **Figure 2**.

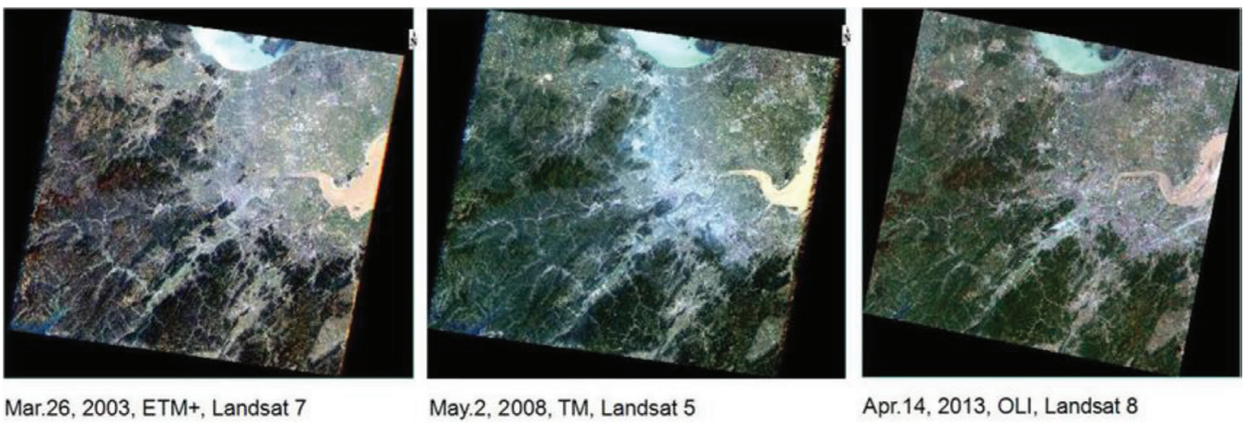

Figure 1. The original image data of study area.

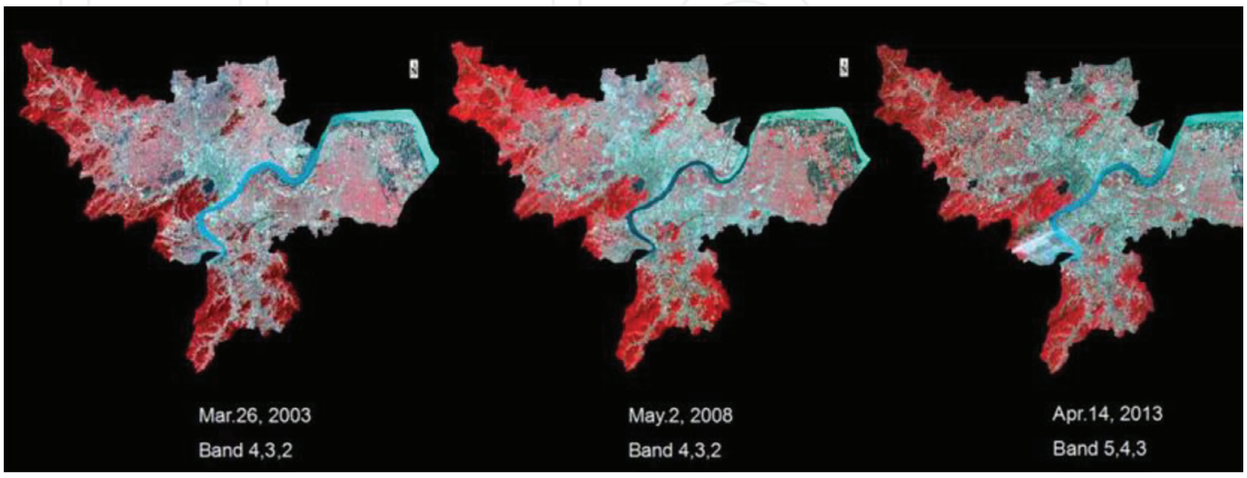

Figure 2. Prepared map combined with different band.

2.3. Method selecting

The most common ways to retrieve land surface temperature (LST) via remote sensing approaches can be summarized into four methods: (1) image-based method (IBM); (2) radiative transfer equation (RTE) also are called atmospheric correction method; (3) Qin et al.'s mono-window algorithm (MWA) [12] and (4) Jiménez-Muñoz and Sobrino single-channel algorithm (SCA) [13].

According to the literature review, it can be found that, using IBM to retrieve LST has less dependent on external factors in real times, and it only takes the impact of land surface emissivity (LSE) into account while ignoring that of atmospheric radiance (AR). When it comes to the RTE and MWA, although they both consider the influence of LSE and AR, excessive external factors which are needed in the equations may decrease the accuracy of the result. In terms of the RTE, those factors include atmospheric sounding database (τ- total atmospheric transmission; L_↑-atmospheric upwelling radiance; L_↓-atmospheric downwelling radiance). In terms of the MWA, those are atmospheric water vapor content and near-surface temperature.

After an overall consideration, SCA was finally chosen by our research team as the major method to conduct our study, since it only needs water vapor content as the absolute external factor, when both considering the impact of LSE and RTE.

3. The single-channel algorithm

3.1. General equations of SCA

In the SCA, LST could be expressed by the general Eq. (1) [13]:

$$T_s = \gamma\left[\frac{1}{\varepsilon}\left(\psi_1 L_{sen} + \psi_2\right) + \psi_3\right] + \delta \tag{1}$$

In this equation, T_s is the land surface temperature in K and γ is parameter according to the Planck function (2) and (3) [13].

$$\gamma = \left\{\frac{c^2 L_{sen}}{T_{sen}^2}\left[\frac{\lambda^4}{c_1} L_{sen} + \lambda^{-1}\right]\right\}^{-1} \tag{2}$$

$$\delta = -\gamma L_{sen} + L_{sen} \tag{3}$$

where $c_1 = 1.09104 \times 10^8\, W\,\mu m^4\, m^{-2}\, sr^{-1}$, $c^2 = 1438.7.7\ \mu mK$, λ refers to the effective wavelength in μm.

Other elements needed in the general equation are ε (the surface emissivity); the at-sensor radiance in $W/(m^{2}{}_{sr\mu m})$; T_{sen} (the at-sensor brightness temperature in K); and the atmospheric parameters ψ_1, ψ_2, and ψ_3.

3.2. Land surface emissivity

Land surface emissivity (ε) can be calculated by the value of the normalized difference vegetation index (NDVI). This index is usually used to detect the growth and coverage of vegetation. NDVI can be expressed by Eq. (4) [14]:

$$NDVI = \frac{NIR - R}{R + R} \tag{4}$$

Based on the study of Zhang in 2006, value of NDVI can be divided into four ranges, and each of the range corresponds to a certain value of land surface emissivity as shown in **Table 1** [14].

3.3. At-sensor radiance

L_{sen} (at-sensor radiance in W/(m^{2} sr μm)) can be achieved by applying radiometric calibration in the data processing software of remote sensing (ENVI 5.1 was used in this research). The equation that used in the software is written as Eq. (5) [15]:

$$L_i = L_{min} + (L_{max} - L_{min}) Q_{dn}/Q_{max} \tag{5}$$

where L_i stands for the at-sensor spectral radiance in $MW \cdot cm^{-2} \cdot sr^{-1} \cdot \mu m^{-1}$; L_{max} and L_{min} refer to the maximum and the minimum at-sensor spectral radiance, respectively; Q_{dn} and Q_{max} are the DN value and the maximum of it in pixel.

3.4. At-sensor brightness temperature

L_{sen} T_{sen} (at-sensor brightness temperature in K) can be transformed from the radiance values of thermal band by Eq. (6) [15].

$$T_{sen} = \frac{K_2}{ln\left(\frac{K_1}{L_{sen}} + 1\right)} \tag{6}$$

where K_1 and K_2 are the thermal calibration constants supplied by the Landsat Project Science Office, which are presented in **Table 2**.

3.5. Atmospheric parameters

ψ_1, ψ_2, and ψ_3 are three different atmospheric parameters and can be obtained in equations of atmospheric water vapor content. For TM/ETM +6 data [13], $\psi_1 = 0.14714w^2 - 0.15538w + 1.1234$, $\psi_2 = -1.1836w^2 - 0.37607w - 0.52894$, and $\psi_3 = 0.00918w^2 + 1.36072w - 0.27514$. For TIRs data [16], $\psi_1 = 0.04019w^2 + 0.02916w + 1.01523$, $\psi_2 = -0.38333w^2 - 1.50294w - 0.20324$, and $\psi_3 = 0.00918w^2 + 1.36072w - 0.27514$.

Based on the study of Jiménez-Muñoz and Sobrino [13], when the value of w is greater than 3 g·cm^{-2}, it will have impacts on the accuracy of the result. In this situation, the original Eq. (7) has been suggested to use to obtain different atmospheric parameters ψ_1, ψ_2, and ψ_3.

NDVI ranges	Main ground covers	Corresponding emissivity
<0.185	Water	0.99
0.185–0.157	Urban used land	0.956
0.157–0.727	Natural ground	1.0094 + 0.047ln(NDVI)
>0.727	High density vegetation	0.985

Table 1. NDVI ranges and corresponding emissivity values.

Sensor	K_1	K_2
Landsat 5 TM band6	607.76	1260.56
Landsat 7 ETM+ band6	666.09	1282.71
Landsat 8 TIRs band10	774.89	1321.80
Landsat 8 TIRs band 11	480.89	1201.14

Table 2. Thermal calibration constants.

$$\psi_1 = \frac{1}{\tau}\psi_2 = -L^{\downarrow} - \frac{L^{\uparrow}}{\tau}\psi_3 = L^{\downarrow} \tag{7}$$

where w is the water vapor content, which can be acquired from Eq. (8).

$$w = w(0)/R_w(0) \tag{8}$$

where $w(0)$ is the water vapor content at 2 m above the ground in the study area. It can be found in the meteorological data recorded in the local observatory. $R_w(0)$ refers to the ratio of near-surface water vapor content of air in the total water vapor content of atmosphere. According to the research by Qin et al. in [17], when the real data are hard to achieve, it can be replaced by standardized atmospheric ratio that is demonstrated in **Table 3**.

HIGHT/km	USA 1976 (Mean)	Tropical	Mid-latitude (summer)	Mid-latitude (winter)	Mean R w (z)
0	0.402058	0.425043	0.438446	0.400124	0.416418
1	0.256234	0.261032	0.262100	0.254210	0.258394
2	0.158323	0.168400	0.148943	0.161873	0.159385
3	0.087495	0.075999	0.074471	0.095528	0.083373
4	0.047497	0.031878	0.038364	0.046510	0.041062
5	0.024512	0.019381	0.017925	0.023711	0.021382
6	0.012846	0.009771	0.009736	0.011514	0.010967
7	0.006250	0.004782	0.005223	0.004092	0.005087
8	0.003132	0.002257	0.002611	0.001471	0.002368
9	0.001049	0.000954	0.001315	0.000587	0.000976
10	0.000358	0.000349	0.000616	0.000238	0.000390
11	0.000142	0.000104	0.000185	0.000060	0.000123
12	0.000055	0.000032	0.000044	0.000026	0.000039
13	0.000023	0.000008	0.000009	0.000016	0.000014
14	0.000009	0.000004	0.000004	0.000011	0.000007
15	0.000006	0.000002	0.000002	0.000008	0.000004

Table 3. Water vapor content distribution by height of atmosphere.

4. Results and discussion

4.1. Land surface temperature distribution in Hangzhou

Based on **Figures 3** and **4**, it can be found that LST of Hangzhou has changed dramatically during the research period (in 2003, 2008, and 2013). In 2003, the mean temperature concentrated in the temperature ranging between 15 and 25°C. Higher temperature (over 20°C) appeared more in the central and west area, such as Yuhang district, Xihu district, the central three districts (i.e., Gongshu district, Jianggan district, and Shangcheng district), and the most part of south-western Xiaoshan district.

When it comes to 2008, compared to 2003, the mean temperature generally increased 5°C in this year, and the higher temperature moved slightly toward east area. The LST increased severely in 2013. Area of temperature in the range of 25–30°C expanded significantly. Higher temperature almost covered the whole Hangzhou city and extreme high temperature demonstrated in the central area aside by the Qiantang River evidently. However, it should be noted that the northwest corner of Xihu district had covered by cloud in that day, so the result of that area is inaccurate (**Table 4**).

4.2. Calculation of urban thermal field variance index

The urban thermal field variance index (UTFVI) is commonly used to express the urban heat island effect. It can be calculated by Eq. (9) [18]:

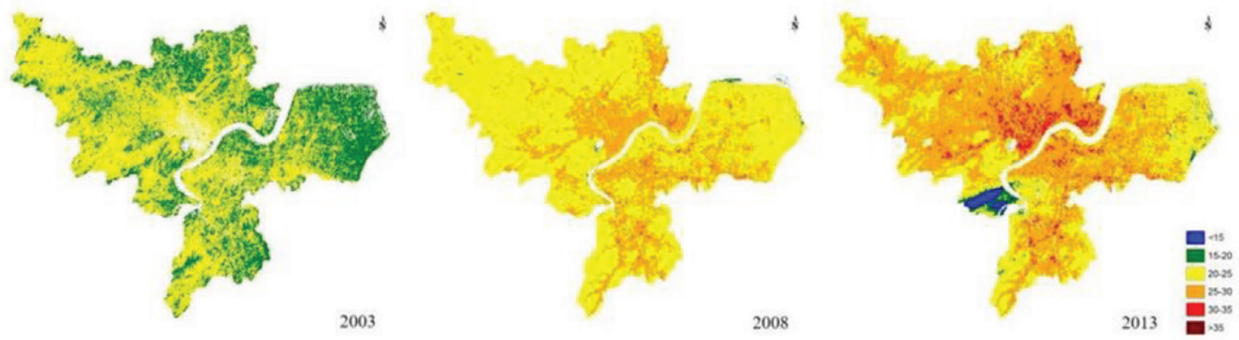

Figure 3. Land surface temperature of Hangzhou in 2003, 2008, and 2013 (°C).

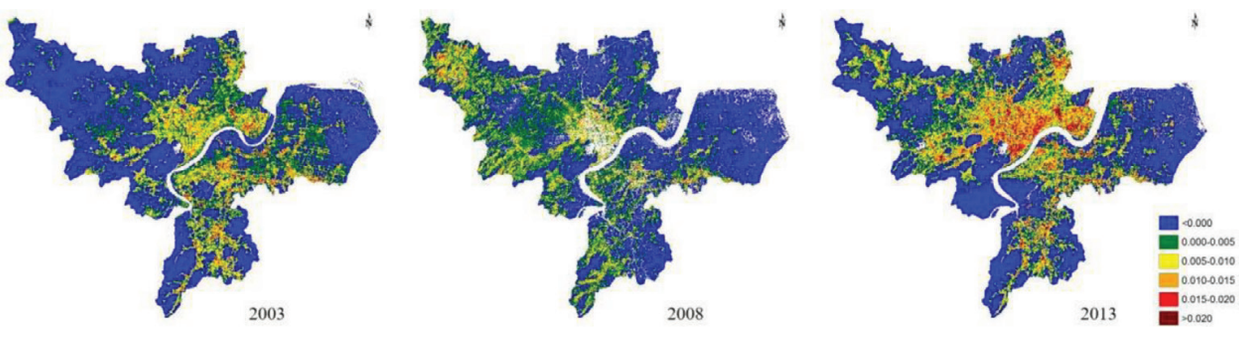

Figure 4. UTFVI of Hangzhou in 2003, 2008 and 2013.

Year	LST (Min)	LST (Max)	LST (Mean)	Stdev
2003	273.541595	309.538513	293.388575	1.683309
2008	285.579773	314.425720	297.305008	1.852384
2013	271.901184	316.897858	298.611333	3.077064

Table 4. Land surface temperature of Hangzhou in 2003, 2008, and 2013 (°C).

$$\text{UTFVI} \frac{T_s - T_{mean}}{Ts} \quad (9)$$

where T_s is the LST in certain point of the map and T_{mean} is the corresponding mean temperature of the whole area.

In order to illustrate the level of urban heat island effect more clearly, the result of UTFVI can be divided into six categories as shown in **Table 5**, and each category is corresponded to a fixed ecological evaluation index (EEI) [18]. The result of UTFVI is shown in **Figure 4**. It can be seen that, UTFVI shows a same pattern of variation as the LST during the given period in Hangzhou city. The urban heat island phenomenon was shown more evidently in 2013, with large area in the central city present extreme high value of UTFVI (over 0.010). Correspondingly, the ecological evaluation index also got worse in this year.

4.3. Change of urban heat island intensity

Urban heat island intensity is defined by Iain D. Stewart as a simultaneous "urban-rural" temperature difference, with "rural" understood as the open countryside and "urban" as the built-up environment of the city [19], which is an index to measure the urban heat island effect.

Some calculation methods have been used in urban heat island study. One is using the difference between typical temperature of rural area and typical highest temperature of urban area [20], which is not easily used because it is difficult to find a meteorological station in rural area in natural situation that has not been impacted by cities. Another is to define the difference of several average temperatures between urban and rural area [21]. This method is widely used

Urban thermal field variance index	Urban heat island phenomenon	Ecological evaluation index
<0	None	Excellent
0.000–0.005	Weak	Good
0.005–0.010	Middle	Normal
0.010–0.015	Strong	Bad
0.015–0.020	Stronger	Worse
>0.020	Strongest	Worst

Table 5. UTFVI and its corresponding EEI.

because it is easy to calculate, however, it cannot reflect the highest rising temperature as it uses the average temperature as measure index. These methods are not easy to measure and compare because they are limited by materials and measure conditions. To avoid these disadvantages, two concepts have been introduced in this research to measure urban heat island intensity.

4.3.1. The highest urban heat rising temperature

The highest UHI rising temperature is the difference between the highest temperature of city center and average temperature of rural area. Eq. (10) [22] can be written as:

$$max\,\Delta T_{ij} = T_{ij} - \acute{T}_R \tag{10}$$

where ΔT_{ij} is the UHI intensity of position ij, T_{ij} is the surface temperature of position ij, and $\acute{T}_R$ is the average temperature of 32 positions in rural area in eight directions.

The results of the highest UHI rising temperature are shown in **Table 6** and **Figure 5**, which reflect the trend that the highest UHI rising temperature is increasing year by year. In the first 5 years, the change is not so apparent and from the period 2008 to 2013, there is a rapid growth and the temperature increased by approximately 2.7°C.

4.3.2. The total amount of urban heat island rising temperature

Another index is the total amount of UHI rising temperature, which reflects the total rising amount of temperature that UHI effects on cities in certain spatial resolution. In order to calculate the total amount of UHI rising temperature, Eq. (11) [22] can be used as:

$$T = \frac{a \times \sum_{j=1}^{m} \sum_{i=1}^{n} x_{ij}}{10000} \tag{11}$$

where T is Total amount of UHI rising temperature (°C·ha), x_{ij} is UHI intensity of position ij, and a is the area of each grid, which is 900 m^2 in this research.

Table 7 and **Figure 6** indicate the calculation result and change of the total amount of UHI rising temperature from 2003 to 2013. It is significant that overall the total amount of UHI rising temperature grows annually from 168681.2°C·ha in 2003 to 447284.8°C·ha in 2013, which is more than doubled. Another change trend is that from 2003 to 2008, the temperature showed a sharp increase, and in the last 5 years, the increasing speed was slowed down, which is opposite to the change of the highest UHI rising temperature. Compared with the change of two concepts,

	2003	2008	2013
Average temperature of rural area (°C)	17.41	26.77	25.4
Highest temperature of city center (°C)	28.67	38.06	39.39
Highest UHI rising temperature (°C)	11.24	11.29	13.99

Table 6. Result of the highest UHI rising temperature.

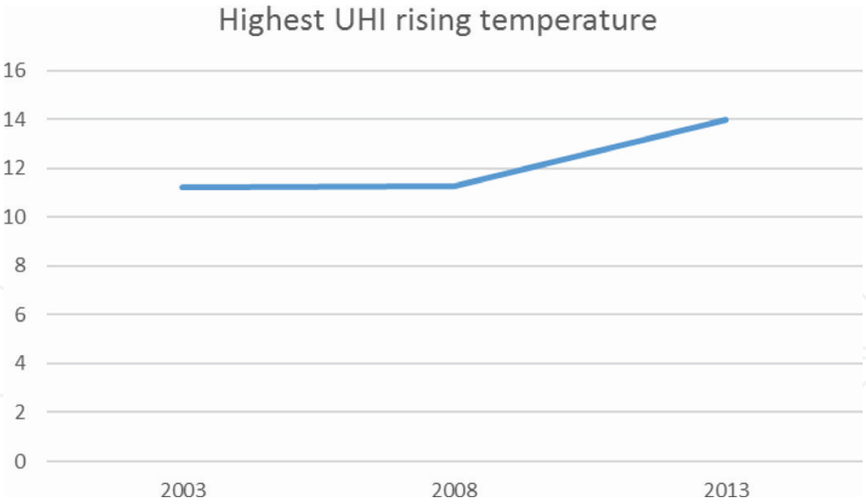

Figure 5. Change of the highest UHI rising temperature.

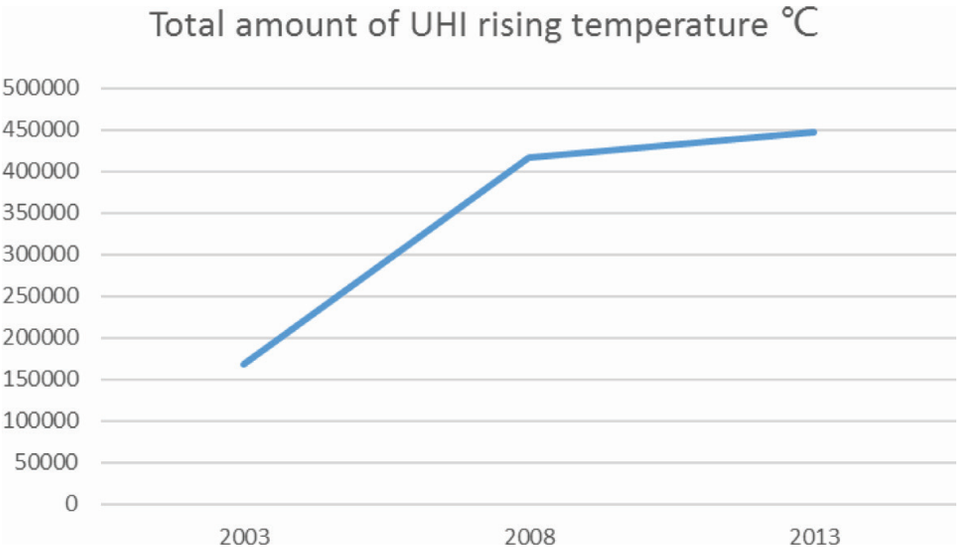

Figure 6. Change of the total amount of UHI rising temperature.

	2003	2008	2013
Sum of UHI intensity (°C)	1874235.59	4634287.11	4969830.97
Total amount of UHI rising temperature °C·ha	168681.2	417085.8	447284.8

Table 7. Result of the total amount of UHI rising temperature.

it can be found that in the first 5 years, the total amount of UHI rising temperature rose in high speed although the highest UHI rising temperature did not change a lot. In the rest years from 2008 to 2013, the change of the total amount of UHI rising temperature had been controlled and the growing speed was slowed down; in contrast, the highest rising temperature increased rapidly, which demonstrates that the temperature difference had been further expanded.

4.3.3. The urban heat island intensity

To define the differences of urban heat island intensity between 3 years, the difference between the temperature of each grid and the average temperature of rural area, which is chosen in eight directions, is used as the measurement. **Figure 7** and **Table 8** demonstrate the change of urban heat island intensity from 2003 to 2013. It can be found in figures and table that the most obvious change happened in the first 5 years as the max temperature difference increased from 11.25 to 21.09°C, and the average temperature difference increased nearly three times from 0.5 to 1.24°C.

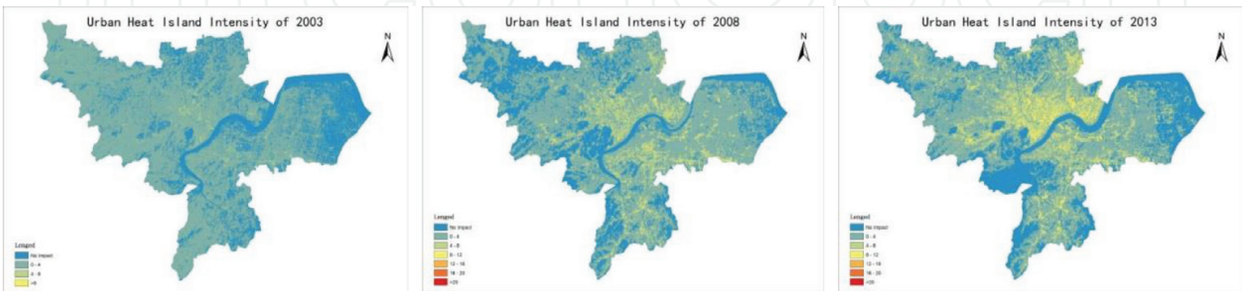

Figure 7. (a) Urban heat island intensity of Hangzhou in 2003; (b) urban heat island intensity of Hangzhou in 2008; and (c) urban heat island intensity of Hangzhou in 2013.

	2003	**2008**	**2013**
Max temperature (°C)	11.25	21.09	22.13
Average temperature (°C)	0.5	1.24	1.33

Table 8. Change of urban heat island intensity of Hangzhou from 2003 to 2013.

		UHI intensity	**NDVI**	**NDBI**
UHI intensity	Pearson correlation	1	−0.872 **	0.682**
	Sig. (two-tailed)		0.000	0.000
	N	300	300	300
	Pearson correlation	−0.872**	1	−0.799**
NDVI	Sig. (two-tailed)	0.000		0.000
	N	300	300	300
	Pearson correlation	0.682**	−0.799**	
NDBI	Sig. (two-tailed)	0.000	0.000	
	N	300	300	300

**Correlation is significant at the 0.01 level (two-tailed).

Table 9. Correlations between UHI intensity and NDVI and NDBI index.

4.4. Response mechanism of urban heat island

The normalized difference vegetation index (NDVI) is a graphical indicator that usually be used to examine whether the object being observed contains live green vegetation or not through remote sensing measurements [23]. The normalized difference build-up index (NDBI) "highlights urban areas where there is characteristically a higher reflectance in the shortwave-infrared (SWIR) region, compared to the near-infrared (NIR) region [24]." Based on the previous research, urban heat island effect is impacted by plants and urban build-up area [24–28], so in this research, NDVI and NDBI have been selected to investigate the response mechanism of urban heat island effect.

In order to calculate the correlations between UHI intensity and NDVI and NDBI index, 300 sampling points had been chosen from high-temperature area, mid-temperature area and low-temperature area of data of 2008. The analysis of correlation is shown in **Table 9**.

Based on the study, it is significant that the urban heat island effect is impacted by NDVI and NDBI, and the NDVI has negative correlation with UHI intensity, while NDBI has positive correlation. This finding of response mechanism of UHI could provide guide to urban planners about how to control the urban heat island effect through planning and design tools.

5. Conclusion and limitation

It is significant that the area in Hangzhou which is impacted by urban heat island effect is expanded annually, and another point that should be mentioned is that the highest UHI rising temperature and total amount of UHI rising temperature show a rapid growth in past 10 years from 2003 to 2013. These changes indicate that Hangzhou is facing a big challenge caused by climate change and urban heat island effect which would have negative impact on people's lives and economic growth.

Based on the liner regression analysis, the NDVI is negative correlated to UHI intensity, and in contrast, NDBI has the positive correlation with UHI intensity. As the UHI intensity has such close correlation with NDVI and NDBI index, two suggestions have been supposed to decrease the urban heat island effect. The first one is greenery design which means that government should encourage developers to design green roof, green pavement, and so on. Another strategy is to optimize the urban morphology, such as mix the green land with building area. These two strategies can decline the UHI intensity by spread NDVI index or drop down the NDBI index.

Nevertheless, we only measure the 3 years' UHI intensity due to the limited time and resources, it is almost certain that more years' data can reflect the change clearer. Another limitation is that only NDVI and NDBI have been taken into assessment. Urban heat island is a thematic effect that is caused by a various kind of factors. Further elements can be added in future study that may reflect the response mechanism better.

Acknowledgements

The data from the website of USGS and from the local government of Hangzhou are highly appreciated. This research was jointly supported by the "2015 Jiangsu Shuangchuang Program," the "National Key Research and Development Program of China (Project Ref. No. 2016YFC1402003)," and the National Foundation of Natural Science of China (No. 41506106).

Conflicts of interest

The authors declare no conflict of interest.

Author contributions

Siqiang Wang and Yuanzhi Zhang conceived and designed the experiments, analyzed the data and wrote the chapter; Meng Xiang and Yanan He performed the experiments; Xia Lu improved the data analysis; and Jin Yeu Tsou and X. San Liang contributed to reagents/materials/analysis tools.

Author details

Siqiang Wang[1], Meng Xiang[1], Yanan He[1], JinYeu Tsou[1], Yuanzhi Zhang[1,2]*, X. San Liang[2] and Xia Lu[3]

*Address all correspondence to: yuanzhizhang@cuhk.edu.hk

1 Center for Housing Innovations, The Chinese University of Hong Kong, Shatin, New Territories, Hong Kong

2 School of Marine Sciences, Nanjing University of Information Science and Technology, Nanjing, Jiangsu Province, China

3 Faculty of Surveying and Mapping, Huaihai Institute of Technology, Lianyungang, China

References

[1] Santamouris M. Energy and Climate in the Urban Built Environment. Oxford, UK: Routledge, Taylor & Francis Group; 2013. 410p

[2] Oke TR, Johnson GT, Steyn DG, Watson ID. Simulation of surface urban heat islands under "ideal" conditions at night part 2: Diagnosis of causation. Boundary-Layer Meteorology. 1991;**56**:339-358

[3] Kolokotroni M, Ren X, Davies M, Mavrogianni A. London's urban heat island: Impact on current and future energy consumption in office buildings. Energy and Buildings. 2012;**47**:302-311

[4] Adams MP, Smith PL. A systematic approach to model the influence of the type and density of vegetation cover on urban heat using remote sensing. Landscape and Urban Planning. 2014;**132**:47-54

[5] Senanayake IP, Welivitiya WDDP, Nadeeka PM. Remote sensing based analysis of urban heat islands with vegetation cover in Colombo city, Sri Lanka using Landsat-7 ETM+ data. Urban Climate. 2013;**5**:19-35

[6] Huang MF, Xing X, Wang PJ, Wang C. Comparison between three different methods of retrieving surface temperature from Landsat TM thermal infrared band. Arid Land Geography. 2006;**29**:132-137

[7] Rinner C, Hussain M. Toronto's urban heat island—Exploring the relationship between land use and surface temperature. Remote Sens. 2011;**3**(6):1251-1265

[8] Chen W, Zhang Y, Gao W, Zhou D. The investigation of urbanization and urban heat island in Beijing based on remote sensing. Procedia - Social and Behavioral Sciences. 2016;**216**:141-150

[9] Liu L, Zhang Y. Urban heat island analysis using the Landsat TM data and ASTER data: A case study in Hong Kong. Remote Sensing. 2011;**3**:1535-1552

[10] Shen H, Huang L, Zhang L, Wu P, Zeng C. Long-term and fine-scale satellite monitoring of the urban heat island effect by the fusion of multi-temporal and multi-sensor remote sensed data: A 26-year case study of the city of Wuhan in China. Remote Sensing of Environment. 2016;**172**:109-125

[11] Li J, Wang X, Wang X, Ma W, Zhang H. Remote sensing evaluation of urban heat island and its spatial pattern of the Shanghai metropolitan area, China. Ecological Complexity. 2009;**6**:413-420

[12] Qin Z, Karnieli A, Berliner P. A mono-window algorithm for retrieving land surface temperature from Landsat TM data and its application to the Israel-Egypt border region. International Journal of Remote Sensing. 2001;**22**:3719-3746

[13] Jiménez-Muñoz JC, Sobrino JA. A generalized single-channel method for retrieving land surface temperature from remote sensing data. Journal of Geophysical Research-Atmospheres. 2003;**108**

[14] Zhang J, Wang Y, Li Y. A C++ program for retrieving land surface temperature from the data of Landsat TM/ETM+ band6. Computers & Geosciences. 2006;**32**:1796-1805

[15] Zhi Q, Ming Z, Karnieli A, Berliner P. Mono-window algorithm for retrieving land surface temperature from Landsat TM6 data. Acta Geographica Sinica. 2001;**56**(4):456-466

[16] Han-Qiu X. Retrieval of the reflectance and land surface temperature of the newly-launched Landsat 8 satellite. Chinese Journal of Geophysics-Chinese Edition. 2015; **58**:741-747

[17] Qin Z, Li W, Zhang M, Karnieli A, Berliner P. Estimating of the essential atmospheric parameters of mono-window algorithm for land surface temperature retrieval from Landsat TM6. Remote Sensing for Land & Resources. 2003;**2**:37-43

[18] Zhang Y, Yu T, Gu X, Zhang Y, Chen L, Yu S, Zhang W, Li X. Land surface temperature retrieval from CBERS-02 IRMSS thermal infrared data and its applications in quantitative analysis of urban heat island effect. Journal of Remote Sensing-Beijing. 2006;**10**:789

[19] Stewart ID. Measuring the Urban Heat Island Intensity: Challenges with "Urban-Rural" Differentiation and the East Asian City. Available online: http://www.lsgi.polyu.edu.hk/RSRG/resources/News/2nd_ws/abstract/stewart.pdf [Accessed: April 10, 2016]

[20] Lowry WP. Empirical estimation of urban effects on climate: A problem analysis. Journal of Applied Meteorology. 1977;**16**:129-135

[21] LIN X, YU S. Interdecadal changes of temperature in the Beijing region and its heat island effect. Chinese Journal of Geophysics. 2005;**48**:47-54

[22] Huang H, Yun Y, Zhao R. Key parameters in urban form layout for weakening urban heat island intensity and its response mechanism. Tumu Jianzhu Yu Huanjing Gongcheng/Journal of Civil Architectural & Environmental Engineering. 2014;**36**:95-102

[23] Normalized Difference Vegetation Index. Wikipedia 2016. Available online: https://en.wikipedia.org/w/index.php?title=Normalized_Difference_Vegetation_Index&oldid=710783256 [Accessed: March 19, 2016]

[24] Zha Y, Gao J, Ni S. Use of normalized difference built-up index in automatically mapping urban areas from TM imagery. International Journal of Remote Sensing. 2003;**24**:583-594

[25] Kumar D, Shekhar S. Statistical analysis of land surface temperature–vegetation indexes relationship through thermal remote sensing. Ecotoxicology and Environmental Safety. 2015;**121**:39-44

[26] Li X, Li W, Middel A, Harlan S, Brazel A, Turner B. Remote sensing of the surface urban heat island and land architecture in Phoenix, Arizona: Combined effects of land composition and configuration and cadastral–demographic–economic factors. Remote Sensing of Environment. 2016;**174**:233-243

[27] Tian P, Tian G, Wang F, Wang Y. Urban heat island effect and vegetation cover index relation using Landsat TM image. Bulletin of Science and Technology. 2006;**5**:28

[28] Li Y, Zhang J, Gu R. Research on the relationship between urban greening and the effect of urban heat island. Journal of Chinese Landscape Architecture. 2004;**1**:72-75

IntechOpen